SAE Technical Paper 2024-01-2361

Experimental Investigation of Internal and External EGR Effects on a CNG-OME Dual-Fuel Engine

Jost A.-K.[1], Guenthner M.[1], Weigel A.[1]
[1] RPTU University of Kaiserslautern-Landau

Abstract

Dual-fuel engines powered by renewable fuels provide a potential solution for reducing the carbon footprint and emissions of transportation, contributing to the goal of achieving sustainable mobility. The investigation presented in the following uses a dual-fuel engine concept running on biogas (referred to as CNG in this paper) and the e-fuel polyoxymethylene dimethyl ether (OME). The current study focuses on the effects of exhaust gas rebreathing and external exhaust gas recirculation (EGR) on emissions and brake thermal efficiency (BTE).
A four-cylinder heavy-duty engine converted to dual-fuel operation was used to conduct the engine tests at a load point of 1600 min^{-1} and 9.8 bar brake mean effective pressure (BMEP). The respective shares of high reactivity fuel (HRF, here: OME) and low reactivity fuel (LRF, here: CNG) were varied, as were the external and internal EGR rates and their combinations. CNG was injected into the intake manifold to create a homogeneous air-fuel mixture, while OME was introduced as a pilot injection directly into the combustion chamber. Results showed an increase in total hydrocarbons (THC) and carbon monoxide (CO) emissions, while nitric oxide (NOx) emissions were significantly reduced compared to diesel operation. Soot emissions were completely mitigated due to the absence of direct carbon bonds in both CNG and OME. For the initial stage of the study, exhaust gas rebreathing was implemented on only one exhaust valve through a second event lift. For the second part of the study, the second event lift was also installed on the other exhaust valve. At a substitution rate of 50 % CNG, THC emissions could be lowered by up to 35 %, CO emissions by up to 50 % and NOx emissions by up to 18 % with the use of internal EGR. The combination of internal and external EGR reduced emissions even further.

Introduction

The transport sector is responsible for about 25 % of the EU's greenhouse gas emissions. Emissions are well above 1990 levels and are still rising. This threatens to compromise the attainment of the 1.5 K target set by the Paris Agreement. A potential solution which is regularly put forward lies in the introduction of low or zero emission vehicles [1]. This may either be achieved by the (complete) electrification of vehicle drives [2] or by using renewable fuels, mainly from synthetic production. These fuels can be divided into two categories: They can be produced either from biomass (biofuels) or in a power-to-liquid or power-to-gas process using green electrical energy. These so-called e-fuels are typically produced from hydrogen and carbon dioxide (CO_2). The required CO_2 may either be derived from combustion processes or from direct air capture (DAC) [3]. CNG or Liquefied Natural Gas (LNG) are examples for fuels that can be provided both from fossil sources or produced as biofuels as well as e-fuels [4]. This opens up the possibility of easily converting existing LNG or CNG vehicle fleets to renewable fuels. The high energy density of liquid and gaseous fuels are advantageous for applications with a high demand for power and energy. Moreover, these fuels allow to use the existing infrastructure while maintaining similar combustion properties to those of fossil fuels [5]. CNG is easy to transport and to store, combining high availability and low cost [6]. It can be utilized in both spark ignited (SI) and compression ignited (CI) engines, with higher efficiency values observed when used in diesel-like processes. However, the poor auto-ignition properties of CNG require a second, more reactive fuel for CI operation [4; 7]. These processes are usually referred to as “dual-fuel” combustion.

Dual-Fuel Combustion Concepts

Dual-fuel combustion (DFC) technology uses a LRF (e.g. CNG) with high knock resistance and a HRF (e.g. diesel) with good autoignition properties due to its high cetane number [8]. The LRF can be introduced into the intake manifold through port fuel injection (PFI) or injected directly into the cylinder during the intake stroke. This results in the formation of a homogeneous air-fuel mixture [9]. Partially replacing diesel with CNG in dual-fuel operation can simultaneously reduce particulate matter (PM) and NOx emissions [10]. However, dual-fuel engines still provide some challenges when it comes to reducing emissions of THC and CO. In particular, methane slip must be avoided due to its negative climate impact [7; 11; 12].
Many measures to reduce NOx emissions in diesel engines, such as the use of EGR, regularly result in an increase in PM. While dual-fuel operation reduces this effect, it is still not completely eliminated [13]. A potential approach to avoid this trade-off is to employ low temperature combustion (LTC) strategies. LTC may be achieved through a number of different combustion processes, including homogeneous charge compression ignition (HCCI), premixed charge compression ignition (PCCI), Homogeneous Charge Induced Ignition (HCII) and Reactivity Controlled Compression Ignition (RCCI) [10; 14]. The common characteristic of these procedures is the relatively low combustion temperature resulting from distributed lean equivalence ratio values [10]. In the HCCI process, the homogeneous air-fuel mixture can be achieved by early injection of the fuel or by a port fuel injection. In combination with lean equivalent ratios (usually $\lambda \geq 2$) or strong dilution with residual gases, this results in a combustion with remarkably low levels of soot and NOx emissions. However, combustion control in HCCI operation remains a challenge due to the difficulty of controlling both ignition timing and heat release rate (HRR) [15]. Additionally, the ignition timing in HCCI operation is strongly influenced by the temperature level of the intake air. Although this can be effectively controlled in a test bench environment, it becomes a challenge in real-life vehicle operation due to the large number of influencing variables [16]. Bessonette et al. demonstrated that fuels with high cetane numbers are suitable for the

lower load range in terms of their auto-ignition properties, while fuels with low cetane numbers ranging from 27 to 32 are more advantageous for high load points [17]. The main difference between PCCI and HCCI is the slightly delayed injection timing, which results in incomplete homogenization of the fuel-air mixture. In addition to the challenge of controlling combustion, persistently high combustion temperatures can cause increased NOx emissions [18]. Fuel stratification is a technique which may be used for extending combustion duration, which in turn helps controlling the heat release and pressure rise rate during combustion [19]. Kokjohn et al. achieved a homogeneous fuel-air mixture as required for a premixed combustion by using gasoline (introduced through PFI) as the LRF. The HRF was introduced directly into the combustion chamber via two consecutive injections which were separated by around 30 degrees of crank angle (CA). The first injection introduced approximately two-thirds of the diesel fuel mass. The combined premixed charge, together with the two diesel injections during compression, led to a stratification of fuel reactivity [20]. Based on these findings, Kokjohn et al. introduced the term RCCI to refer to this chemically controlled combustion process. Simultaneous reduction of NOx and soot emissions could be achieved through a series of sequential auto-ignition events determined by fuel reactivity and lean conditions during combustion initiation. Furthermore, this process proved to be significantly easier to control and manage in comparison to the HCCI approach. Depending on the load, variable in-cylinder blending of the low and high reactivity fuel is used [15; 16; 20]. Similar to other dual-fuel processes, comparatively high levels of THC and CO emissions were observed. Paykani et al. discovered that using dual diesel injection events instead of a single injection may lower these emissions by up to 40 % and at the same time reduce the pressure rise rate. On the other hand, using direct injection for both fuels is another promising solution. Avoiding wall wetting with early diesel injection remains an ongoing challenge, however [21].

Unlike other dual-fuel processes, HCII performs only one late diesel injection set at 12° before top dead center (BTDC), as shown in a study by Yu et al. [22]. Still, HCII also significantly reduces soot and NOx emissions compared to conventional CI, an effect which is further improved by the use of EGR. For the investigations of Yu et al., gasoline was used as the LRF, leading to an increase in THC emissions as the gasoline share increased. This was attributed to the uniform introduction of the fuel and the subsequent flame quenching and extinction in the crevices.

Influence of external and internal EGR

In order to mitigate the issue of flame quenching in the homogeneous part in the mixture, studies on the effects of increased injection pressure and EGR have been carried out. Chen et al. found that increasing the HRF injection pressure can lower CH_4 and CO emissions at high EGR rates [23]. However, the impact of increased injection pressure on emission reduction proved to be negligible at low EGR rates. With increasing EGR rates, CH_4 and CO emissions also increased while NOx emissions exhibited the opposite behavior. At EGR rates beyond 40 %, combustion became instable. Dev et al. discovered that delayed injection in a CNG-diesel dual-fuel engine can reduce NOx emissions, but result in increased soot and CH_4 emissions [24]. The implementation of cooled external exhaust gas recirculation reduced the maximum heat release and prolonged combustion duration. Furthermore, as in conventional diesel combustion (CDC), high EGR rates resulted in a rise of soot emissions.

To stabilize combustion in a diesel engine, Gonzalez et al. utilized internal EGR through a second exhaust valve lift [25]. They achieved a reduction in THC and NOx emissions by up to 46 % while still facing some limitations due to increasing soot production. Shim et al. explored the effects of hot as well as cooled EGR on mitigating bulk quenching under low load conditions [26]. The investigation found that increasing the charge air temperature through hot EGR and managing the global equivalence ratio are beneficial in this context. According to Mueller et al., using both external and internal EGR in combination reduces CO and CH_4 emissions in dual-fuel operation while maintaining low NOx emissions [27]. However, despite high CNG substitution rates, the issue of soot emissions remained a significant concern at high EGR levels.

Alternative Fuels in Dual-Fuel Combustion

A possible solution to the challenges discussed above is to replace diesel as the HRF by alternative fuels which are unlikely to produce particulate emissions. Polyoxymethylene dimethyl ether (POMDME or "OME") – classified as a C1 oxygenate – is a suitable ignition fuel for this purpose due to its chemical structure $CH_3–O–(CH_2–O)_n–CH_3$. The lack of direct carbon bonds leads to virtually soot-free combustion [28; 29]. OME production can either be achieved by the conversion of methanol and formaldehyde through the intermediate products trioxane and methylal or with the use of an acid catalyst [30]. According to Schmitz et al. [31], an aqueous solution of methanol and formaldehyde offers an opportunity to optimize the process.

The use of OME as an ignition fuel in dual-fuel combustion was investigated by Srna et al. [32]. As a result of the higher cetane number of OME, less HRF was required to control combustion phasing compared to CNG-diesel dual-fuel operation. Hariharan et al. analyzed the impact of injection timing, charge air pressure and rail pressure on a CNG-OME dual-fuel engine [33]. Reducing the charge air pressure decreased CO emissions. Early injection timing, on the contrary, increased CO and THC emissions and reduced engine efficiency while decreasing NOx emissions at the same time. A variation of rail pressure produced no detectable effect on emissions. Duan et al. found that reverse RCCI (R-RCCI) provides an option to lower NOx emissions while maintaining high combustion efficiency [34]. In the case of R-RCCI, the HRF is injected into the intake air, whereas the LRF is introduced directly into the combustion chamber.

Previous investigations carried out by the authors with a similar setup as in the current study already addressed the impact of internal and external EGR in CNG-OME dual-fuel in comparison to CNG-diesel dual-fuel operation [29]. The most significant reduction in THC and NOx emissions was achieved at stoichiometric air-fuel ratio. A slightly lean overall air-fuel equivalence ratio of around 1.22 produced the minimum level of CO emissions, while no soot emissions were detected over the entire operating range.

The aim of the current study is to assess in more detail the impact of both internal and external EGR on a CNG-OME dual-fuel engine. The analysis covers variations of both substitution rate and EGR ratio, evaluating emissions, combustion characteristics, global air-fuel ratio and efficiency. The effects of torque and speed were analyzed at operating points ranging from 4.9 to 14.7 bar BMEP. To carry out the investigation, a non-road diesel tractor engine was converted to dual-fuel operation, and a fully variable valve train was integrated to provide the option of internal EGR through exhaust gas rebreathing (the details of this setup are explained in the subsequent section). Additionally, an adapted piston design with a reduced compression ratio was used in replacement for the original piston of the base engine. During the first phase of the study, the second event lift for the internal EGR was implemented on one of the two exhaust valves, whereas it was installed on both valves for the second part. The analysis also

considers the effect of internal and external EGR on the overall residual gas level.

Experimental Setup

A modified four-cylinder diesel engine manufactured by John Deere was utilized for the experiments. The base engine's technical data is displayed in Table 1. Since the engine uses a two-stage turbocharging system with only one wastegate (solely for the high-pressure stage), the entire exhaust gas flow is transferred to the second turbocharger stage [35].

Table 1. Specifications of the JD4045 base engine

	Value	Unit
Rated Power	130	kW
Rated Speed	2100	min^{-1}
Peak Torque (@1600 min^{-1})	703	Nm
Displacement	4.5	dm^3
Stroke	127	mm
Bore	106.5	mm
Compression Ratio	17.3:1	-
Valves per Cylinder	4	-

A new cylinder head was designed and integrated to enable internal EGR through a second exhaust valve lift. This entailed the modification of the valve train from a single camshaft integrated in the engine block to a completely new design with double overhead camshafts (DOHC). Moreover, the DOHC design features a fully variable valve train (VVT) for both the inlet and the exhaust side. The modification resulted in a reduction of the original engine's compression ratio from 17.3:1 to 16.7:1. In subsequent testing, the intake valve lift remained constant while the exhaust valve lift was varied. In the initial stage of the study, only one exhaust valve (EV1) per cylinder was equipped with the second exhaust valve lift, which was adjustable between 0 and 1.9 mm (the minimum second valve lift is also referred to as "no second event"). The maximum second event (SE) lift is referred to as "full SE". Figure 1 displays the measured valve lifts, starting from firing top dead center (TDC) at 0° CA. The SE valve lift is dependent from the main valve lift which can be adjusted between 8.8 and 5 mm. This range corresponds to the SE lift between 1.9 and 0 mm as already mentioned above. This behavior is illustrated by the red curves displayed in Figure 1. The orange curve shows the valve lift curve for EV2, which consistently performs the maximum valve lift without any SE. The intake valve lift shown in blue can be adjusted continuously between 0 and 7.3 mm. More information concerning the valve train can be found in [36].

In the second stage of the investigation, the second exhaust valve lift was also integrated for the other exhaust valve in order to increase residual gas recirculation. However, in this case the second exhaust valve lift was not varied but instead always used the full main lift and the full second event lift. Due to geometrical limitations of the design, for EV 2 the main lift was 8.4 mm while the second event lift was 1.6 mm. In the Results section, internal EGR on one exhaust valve will be referred to as "EV1 int. EGR" while the second exhaust valve lift on both EVs will be described as "max. int. EGR".

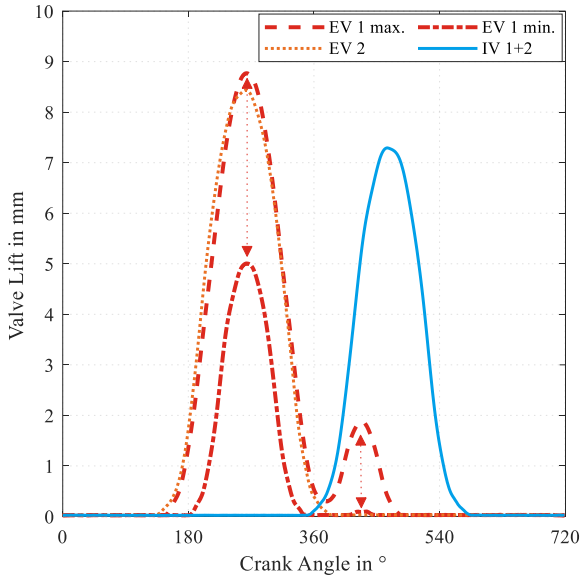

Figure 1. Measured valve train characteristics of the intake and exhaust valves

Another modification was made by applying and implementing a new piston design. Figure 2 displays the two different piston geometries. The base engine's piston has an "omega" type bowl design (blue curve) typical for a diesel engine, while the modified piston bowl is an open crater geometry (red dotted curve). For this layout, the squish gaps were reduced, which in turn led to a further reduction in compression ratio down to 15.8:1. The squish height was not modified, nor was the top ring crevice.

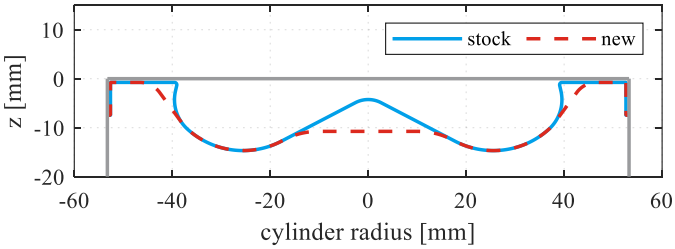

Figure 2. Old (blue) and new (red) piston geometry

In order to enable the standard engine to be operated with dual-fuel combustion, an intermediate flange was fitted between the EGR mixer and the cylinder head. CNG port injection was carried out through four Bosch NGI2 injectors, which were connected to a common CNG rail fixed on top of the intermediate flange.

Achieving a uniform distribution of the LRF between the cylinders proved to be challenging [27; 29]. Therefore, a further adjustment was made by integrating individual cylinder feeds for the LRF using guiding pipes. That allowed the CNG mass flow to be introduced directly in front of the respective inlet valves of all four cylinders. The CNG rail pressure was kept constant at 6.9 bar throughout all of the measurements. The injection quantity and timing for each cylinder was controlled by a Motec M800, while the original engine control unit (ECU) timed the injection of the HRF. The injection timing could only be chosen within predetermined limits of the original engine ECU, which excluded the option of RCCI operation with initial injections required to occur around 50 °BTDC. The quantity was defined by the requested torque and speed and could not be varied manually. The

injected fuel mass was therefore determined by the CNG share and the HRF's lower heating value (LHV) and viscosity. The fuel flow rates were measured by two Endress+Hauser Cubemass C300 Coriolis mass flow meters. The HRF was conditioned to a relative pressure of 400 mbar at a temperature of 40 °C before the high-pressure pump. A calibrated Bosch HRF7 was used to determine the inlet air flow while Kistler 4011 piezoresistive low-pressure transducers were used to measure temperature and pressure on the intake and exhaust manifold side of cylinder 4. The high-pressure indication was recorded with Kistler 6056 piezoelectric pressure sensors with glow plug adapters for each cylinder. The evaluation of these pressure signals was performed with IndiCom software and an AVL Indimodul 621. The crank angle was logged by a Heidenhain ROD 426 crankshaft encoder with a resolution of 0.1 °CA. Thermocouples type N and four wired resistance thermometers were used for temperature recording while Wachendorff ST3708 and ST3808 analog input modules served for logging temperature values. Pressure values were logged with Wachendorff ST3218 analog input modules and recorded by Endress+Hauser pressure sensors. The recorded data was acquired and stored using National Instruments LabVIEW. The torque was applied using a Schenck WT 470 eddy current dynamometer, which was also controlled through the LabVIEW interface. Novotechnik RSC-2841 sensors on the inlet and exhaust eccentric shafts enabled the detection of the valve lifts. For determining PM emissions, the photoacoustic measurement principle was used by an AVL Micro Soot sensor. The gaseous raw emissions as well as the EGR rate were measured by a Horiba MEXA-6000FT Fourier transfer infrared spectrometer in combination with a Horiba Mexa 7170 DEGR emission analyzer. A schematic of the test bench setup is shown in Figure 3.The relevant emission limits for EU stage V for subcategory NRE-v-5 are displayed in Table 2. As no exhaust gas aftertreatment is used, all emissions shown below are raw emissions and not tailpipe emissions

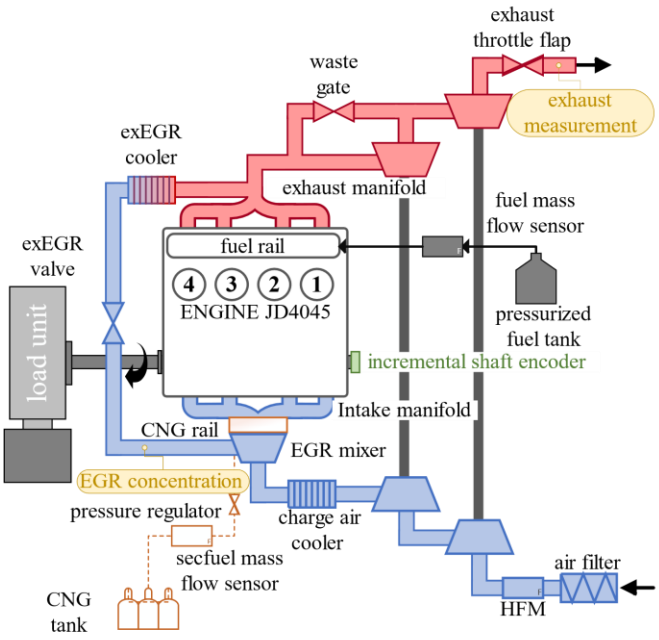

Figure 3. Schematic of the laboratory setup on the engine test bench

Table 2. EU stage V emission limits for engine subcategory NRE-v-5 [37]

Emission	Value	Unit
CO	3.50	g/kWh
UHC	0.19	g/kWh
NO_x	0.40	g/kWh
PM	0.015	g/kWh
PN	1 x 10^{12}	#/kWh

According to Oelschlegel [38], exhaust gas recirculation (EGR) can be introduced either as "additional" or "replaced" EGR, with the possibility of both variants occurring in combination. In the case of replaced EGR, the boost pressure stays within a constant range, resulting in a displacement of part of the fresh air by the recirculated exhaust gas. On the other hand, with additional EGR, the boost pressure is increased to the point where the original fresh air volume is maintained despite the EGR addition. Since the John Deere 4045 engine's intake boost pressure cannot be controlled directly, the recirculated exhaust gas displaces a part of the fresh air volume in the current setup, resulting in an increase of the inlet manifold temperature. Consequently, there is a pressure drop in the inlet pressure, which results in a disproportionate decrease in the availability of oxidizer with increasing external EGR rates.

The fuel properties of the HRF and the LRF used for the investigations are presented in Table 3.

Table 3. Characteristics of the investigated fuels

Parameter	Unit	OME 3-5	CNG
*Cetane/**Methane number	-	73.2*	79.43**
Density (15° C)	kg/m³	1067.1	0.8002
Lower heating value	MJ/kg	19.225	46.968
Oxygen content	% (m/m)	42.60	1.07
Carbon content	% (m/m)	43.80	73.76
Hydrogen content	% (m/m)	8.68	24.16
Nitrogen content	% (m/m)	0.0135	1.01
Sulfur content	mg/kg	< 0.5	-

Methodology

A load point of 1600 min^{-1} and 350 Nm with a BMEP of 9.8 bar was chosen for the investigation discussed below. This load point is relevant in the non-road steady cycle and represents 50 % of the engine's maximum torque. The influence of the amount of external and internal EGR as well as their combination is shown in the Results section. The average center of combustion was kept constant at 8 °CA throughout the measurements. The center of combustion of each individual cylinder may nonetheless vary due to non-uniform distribution between the four cylinders. Since BMEP and speed were kept constant throughout the investigation, the indicated mean effective pressure (IMEP) also varied depending on the substitution and the EGR rate.
To calculate the current external EGR rate, the CO_2 content was measured in the intake system ($c_{CO2,Intake}$), the exhaust system ($c_{CO2,Exhaust}$) and in the environment ($c_{CO2,Ambient}$). The EGR rate (x_{EGR})

for the following investigations was calculated by the CO_2 ratio between intake and exhaust gas side:

$$x_{EGR} = \frac{c_{CO_2,Intake} - c_{CO_2,Ambient}}{c_{CO_2,Exhaust} - c_{CO_2,Ambient}} \cdot 100\,\% \quad (1)$$

The chemical energy of the low reactivity fuel divided by the total chemical energy of both fuels defines the substitution rate $x_{Subst.}$:

$$x_{Subst.} = \frac{\dot{m}_{CNG} \cdot LHV_{CNG}}{\dot{m}_{CNG} \cdot LHV_{CNG} + \dot{m}_{OME} \cdot LHV_{OME}} \cdot 100\,\% \quad (2)$$

The air-fuel equivalence ratio (λ) of both fuels was calculated in dependence of the substitution rate. It is described by the addition of the product of fuel mass flows and the stochiometric air fuel-ratio (AFR_{ST}) of the corresponding fuel in relation to the inlet air mass flow:

$$\lambda = \frac{\dot{m}_{air}}{\dot{m}_{CNG} \cdot AFR_{ST,CNG} + \dot{m}_{OME} \cdot AFR_{ST,OME}} \quad (3)$$

For further analysis of the measurement results, a three-pressure analysis (TPA) model was established in GT-POWER (cf. Figure 4). The necessary input data was obtained from piezoresistive low-pressure transducers positioned in the intake and exhaust manifold of cylinder 4 and from the high-pressure sensor of the same cylinder. Moreover, a 3D-CFD model was set up for the purpose of more extensive analysis, which is continuously validated with the experimental data. This model aims at a better understanding of the effects of in-cylinder flow and of the reaction kinetics of OME in dual-fuel combustion. Additional gas exchange characteristics, such as swirl levels and discharge coefficients of the valves, were acquired by 3D-CFD simulations during a previous project [36; 39].

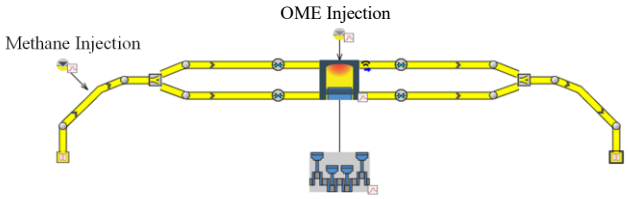

Figure 4. GT-POWER TPA model for cylinder 4

Results and Discussion

The experimental results presented below illustrate the impact of substitution rate as well as external and internal EGR on emissions, efficiency and combustion characteristics for the studied medium-load operating point with an engine speed of 1600 min^{-1} and a brake torque of 350 Nm. All results were obtained applying the methodology described in the previous section.

Influence of the substitution rate

For the investigations, the substitution rate was varied in increments of 25 % up to 75 %, complemented by an additional step at 90 % CNG share. The upper diagram in Figure 5 illustrates the BSTHC and BSCO emissions as a function of the substitution rate. THC emissions persistently increased as the substitution rate was raised, while CO emissions peaked at substitution rates between 50 % and 75 % and then fell again for 90 % substitution rate. This can be explained by the decreasing overall combustion efficiency at high substitution rates, leading to less hydrocarbons being partly or completely oxidized. This shifts the carbon balance towards unburned hydrocarbons instead of (partly or fully) oxidized carbon such as CO or CO_2, which resulted in the observed increase in unburned HC and decrease in CO. It needs to be underlined that this cannot be attributed to a general lack of oxygen, since the global air-fuel equivalence ratio is still larger than λ=2 in this case. With higher substitution rates, however, the chance of misfiring due to flame quenching or extinction in the squish gap increases drastically. This results in increasing cyclic variations and therefore higher methane slip (THC) and CO emissions [40]. Since the typical omega-type bowl design of a diesel engine is not well suited for the combustion of a homogeneous mixture, higher substitution rates also resulted in an increasing share of unburned hydrocarbons from the squish gap and the top ring crevices. Additionally, the lower graph in Figure 5 displays the air-fuel equivalence ratio λ as a function of the substitution rate, together with the development of brake thermal efficiency for the same variation. As the proportion of CNG increased, lambda decreased continuously due to the injected CNG partly displacing the aspirated air. BTE increased for substitution rates up to 50 % CNG. For substitution rates larger than 50 %, unburned hydrocarbons were excessively increasing, which resulted in a reduction of efficiency. Obviously, for substitution rates beyond 50 % the temperature required for the oxidation of methane can no longer be ensured throughout the entire in-cylinder volume during combustion, which resulted in high methane slip when running the engine without EGR. This is particularly relevant for substitution rates of 75 % and more, exhibiting an over-proportional increase in THC emissions and a corresponding drop in combustion efficiency.

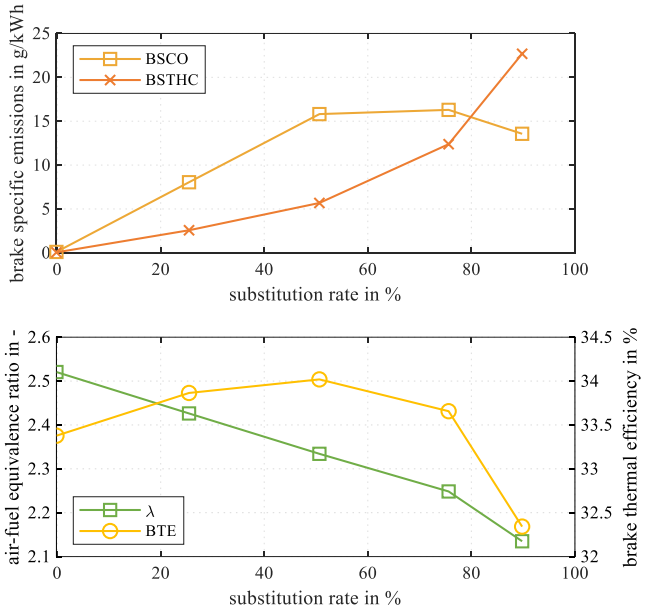

Figure 5. BSTHC and BSCO emissions, λ and BTE for substitution rates between 0 % and 90 % CNG share (1600 min^{-1}, 350 Nm without EGR)

Figure 6 shows a decrease in both CO_2 emissions and NOx emissions as the substitution rate increased. Methane as the main component of CNG has a more favorable H/C-ratio compared to OME. As a result, CO_2 emissions were continuously decreasing with increasing CNG substitution rate.

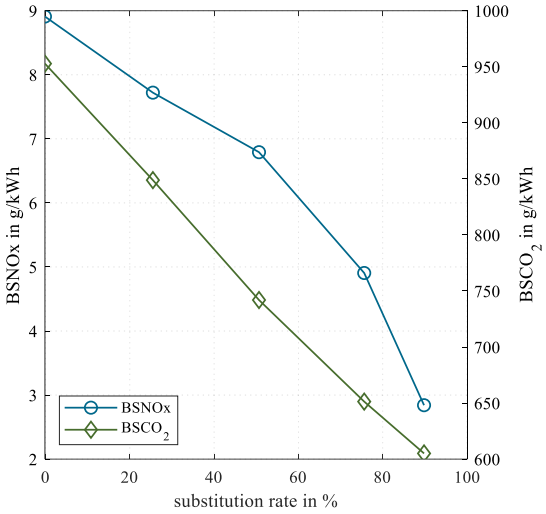

Figure 6. BSNOx and $BSCO_2$ emissions for substitution rates between 0 % and 90 % CNG share (1600 min^{-1}, 350 Nm without EGR)

Krishnasamy et al. [41] show a soot and NOx formation plot in dependence of the local equivalence ratio and the temperature. The original version by Kanimoto et al. [42] has been discussed many times and extended several times to include different combustion processes [20; 41]. It shows that for dual-fuel operation with diesel, the LTC is located in a range of low soot and low NOx emissions. The correlation of NOx reduction due to the transition from diffusion-flame combustion to lean flame front combustion has been discussed in previous publications [27]. The formation of NO through the Zeldovic mechanism becomes relevant only at temperatures beyond 2200K. At a temperature of 1800 K, on the contrary, the reaction progresses 7 to 8 orders of magnitude slower. Raising the temperature by a factor of two results in an increase in NO emissions by a factor of 1000 [43]. An indication for a LTC process is the decrease of the NO to NO_2 ratio (referred to as x_{NOx}) as the reaction shifts from predominant NO production to higher NO_2 shares. The NO/NO_2 ratio was calculated as follows:

$$x_{NOx} = \frac{BSNO}{BSNO_2} = \frac{BSNO\ \left(M = 30.01 \frac{g}{mol}\right)}{BSNO_2\ \left(M = 46.01 \frac{g}{mol}\right)} \qquad (4)$$

As defined through the exhaust standard EU stage V, the emissions of NO are multiplied with the molar mass of NO_2 when converting the concentration of NO emissions in ppm to brake specific emissions for BSNOx (for the emission standard, it is assumed that the emitted NO will be oxidized to NO_2 in the ambient). Therefore, the measured NOx emissions were slightly higher than the sum of the NO and the NO_2 emissions. The molar masses used for the calculation are provided in parentheses in the above formula. The BSNO emissions, however, were calculated using the actual molecular weight of NO. At lower flame temperatures, NO_2 is mostly formed by the reaction of $NO+HO_2$. However, due to insufficient mixing and the overall slower combustion, NO_2 is not able to react in the reverse direction to form NO [43] and therefore remains in the exhaust gas as NO_2. With higher substitution rates, $BSNO_2$ rose while BSNO decreased. This relation is shown in Figure 7. In OME-only operation, the x_{NOx} ratio was slightly larger than 10, while at 25 % substitution rate, it was already at 1.3. x_{NOx} then decreased linearly with increasing substitution rate, down to a ratio of 0.66 at 90 % CNG.

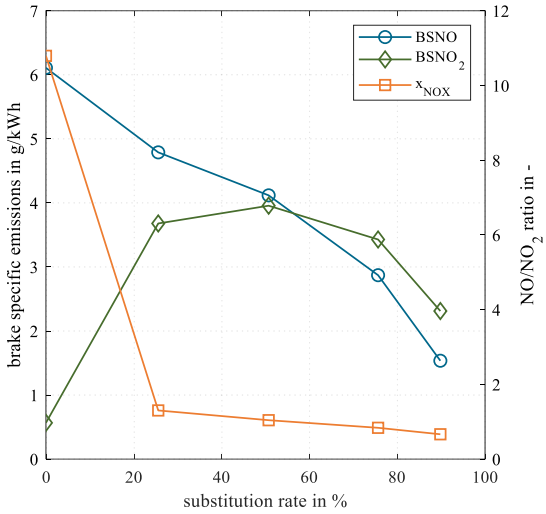

Figure 7. BSNO, $BSNO_2$ emissions and the NO/NO_2 ratio for substitution rates between 0 % and 90 % CNG share (1600 min^{-1}, 350 Nm without EGR)

Overall, NOx emissions can be reduced from slightly below 9 g/kWh without CNG to less than 3 g/kWh.
Figure 8 shows the in-cylinder pressure at bottom dead center (BDC) after gas exchange and the exhaust gas temperature, plotted as a function of the substitution rate. Both values decreased steadily until a substitution rate of 75 % was reached, from which they started to rise again.

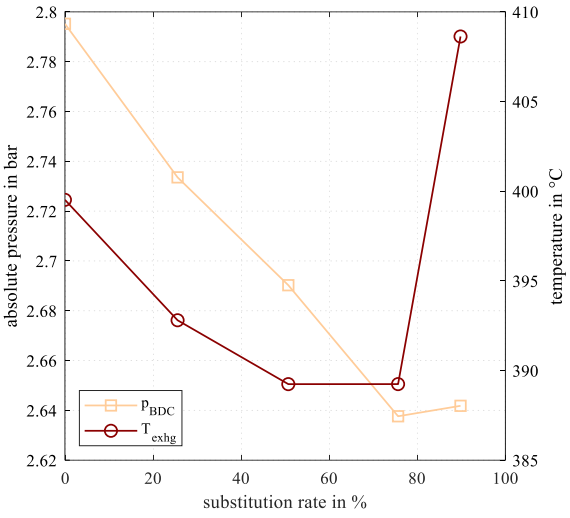

Figure 8. Bottom dead center pressure and exhaust temperature for substitution rates between 0 % and 90 % CNG share (1600 min^{-1}, 350 Nm without EGR)

To help explain this finding, Figure 9 shows the ignition delay and combustion duration as a function of the substitution rate. Due to a reduction of the combustion duration up to a substitution rate of 50 %, the exhaust gas temperature is reduced, which negatively affects the turbocharger performance and thus lowers BDC pressure. Consequently, BDC pressure dropped up to a substitution rate of 75 % before rising again due to the increased exhaust gas temperature caused by the longer combustion duration. Both ignition delay and combustion duration decrease up to a 50 % CNG substitution level and subsequently increase again. The combustion duration with 75 %

CNG substitution rate is longer compared to 90 % CNG substitution. Due to the higher ignition delay at 90 % CNG substitution rate, the introduced OME is rapidly converted, leading to a steep initial heat release rate, as obvious from Figure 10.

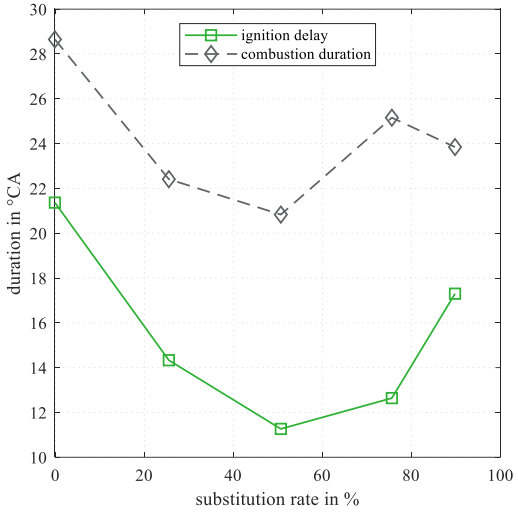

Figure 9. Ignition delay and combustion duration for substitution rates between 0 % and 90 % CNG share (1600 min^{-1}, 350 Nm without EGR)

Figure 10 shows the apparent heat and the cumulative heat release rates of cylinder 4. The heat release rates were calculated according to the AVL Indicom software documentation. The polytropic coefficient for diesel and gaseous-fuel engines used was 1.37 during compression and 1.30 for expansion. The combustion duration can also be seen in the cumulative heat release rates in the lower part of Figure 10. Here, a steeper slope is an indicator of more rapid combustion. The steepest slope is obtained with 50 % substitution rate (yellow curve), while the case without CNG (blue) exhibits the least steep curve and therefore the longest combustion duration. This can also be seen in the apparent heat release rate (AHRR). The blue curve describes the operating point without CNG with a reduced premixed combustion phase followed by a nearly constant low-level heat release. This prolonged diffusion flame combustion is caused by an extended injection duration due to the reduced LHV of OME. In comparison to diesel, more than twice the mass of OME is necessary to introduce same amount of energy. Since the goal of the measurements was to achieve a constant center of combustion at 8 °CA ATDC, the injection timing for OME-only operation was set at 14.2 °CA BTDC. The early injection timing and therefore low pressures and temperatures are responsible for the long ignition delay in OME-only operation. The transition from premixed to flame-front combustion is smooth at substitution rates between 25 and 50 % CNG share. At 75 % substitution rate (green curve), the first peak describes the premixed combustion transformed into a mixture of diffusion flame and flame front combustion. At the heat release peak at 2.5 °CA ATDC, the OME injection ends and the diffusion flame combustion transitions into a flame front combustion. At 90 % substitution rate, a short decrease in the apparent heat release can be observed at 5 °CA BTDC due to the ignition delay of the bulk mixture. This point also marks the end of the OME injection. The more CNG is introduced, the more the diffusion flame combustion changes to a mixture of diffusion flame and flame front combustion.

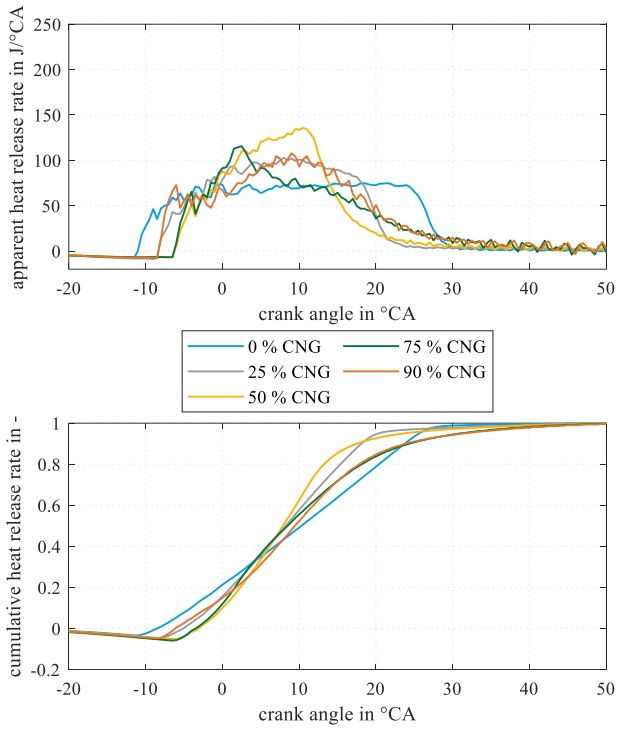

Figure 10. Apparent and cumulative heat release rates for cylinder 4 for substitution rates between 0 % and 90 % CNG share (1600 min^{-1}, 350 Nm without EGR)

In Figure 11, the calculated temperature of the burned zone as a function of the substitution rate is presented. At 90 % CNG substitution rate, combustion starts at a lower temperature level compared to 75 % CNG, but decreases less rapidly. The highest temperature, combined with the steepest decrease, was found at 0 % CNG. This operating point also has the largest ignition delay and the longest combustion duration.

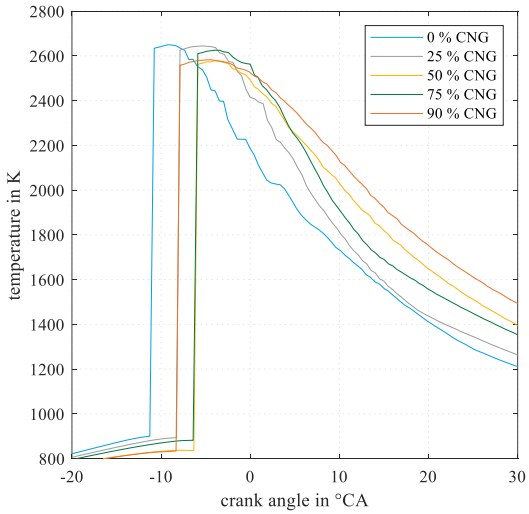

Figure 11. Effect of CNG substitution rate on the progression of in-cylinder temperature of the burned zone according to TPA simulation at 0 % EGR (1600 min^{-1}, 350 Nm without EGR), calculated values

Influence of the substitution rate on EGR effects

The following section discusses the various effects of EGR depending on the CNG share. Based on the operation without EGR discussed above, the (variable) second event used for internal EGR was first applied on only one exhaust valve ("EV1 int. EGR"), before it was implemented on both valves ("max. int. EGR"). Also, operation with 20 % external EGR and the combination of max. internal EGR with 20 % external EGR has been investigated. Figure 12 shows the BSTHC emissions in the upper graph and the BSCO emissions below as a function of the CNG substitution rate. As the CNG substitution rate increased, there was a concurrent rise in THC emissions due to the release of more unburned methane. This correlation could be mitigated with the utilization of EGR. The recirculated exhaust gas generally raises the mixture temperature before combustion while also reducing peak combustion temperature. The temperature in the combustion chamber remained above the temperature required for the oxidation of methane for an extended period of time, leading to reduced unburned hydrocarbon emissions. In this regard, the impact of internal EGR was higher than that of external EGR. This is due to the fact that the (uncooled) rebreathed internal EGR has a more significant effect on in-cylinder temperature than externally recirculated, cooled EGR. CO emissions followed this trend equally but increased when combining internal and external EGR. This is due to local oxygen shortage resulting from the low global air-fuel equivalence ratio (Figure 18 further down).

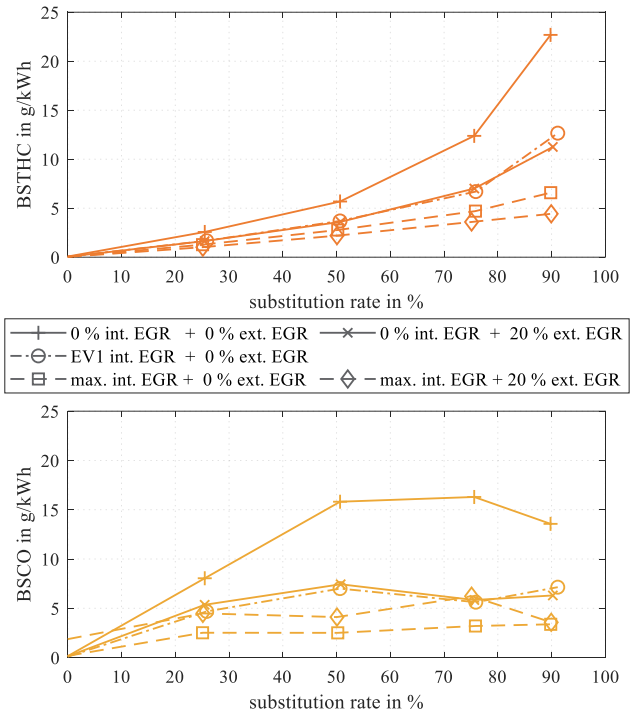

Figure 12. BSTHC and BSCO emissions for internal and external EGR variation at substitution rates between 0 % and 90 % CNG share (1600 min^{-1}, 350 Nm)

Since the temperatures were kept at a higher level for a longer period of time, NOx emissions might be expected to increase with higher EGR rates. However, this is not the case due to the higher impact of the dilution effect of the EGR. According to Heywood [44], the most important contribution is the absolute heat capacity of the charge mixture inside the cylinder. Additionally, with increasing EGR rates, the heat capacity is rising due to the increased share of triatomic molecules (CO_2, H_2O) in the recirculated exhaust gas. Figure 13 shows the progression of NOx emissions in the upper diagram and CO_2 emissions below. Since internal EGR also increased the in-cylinder charge temperature prior to combustion, the density of the charge is reduced and thus also the pressure peak during combustion [27]. The flame front temperature decreased with increasing EGR and substitution rate, resulting in a reduction of NOx emissions. In addition, the air mass in the cylinder decreased due to the higher exhaust gas content and methane fraction in the cylinder charge, further reducing NOx formation. CO_2 emissions dropped both as the CNG share and as the EGR rate increased. The positive influence of the substitution rate can be attributed to the advantageous H/C ratio of CNG. The influence of EGR is correlated with the gas exchange loss in this context. Internal EGR produced a stronger impact on the reduction of the gas exchange loss, which is why CO_2 emissions could be further reduced through the use of internal EGR. Gas exchange losses for the operating point with max. int. EGR were almost identical to the same operating condition with additional 20 % ext. EGR.

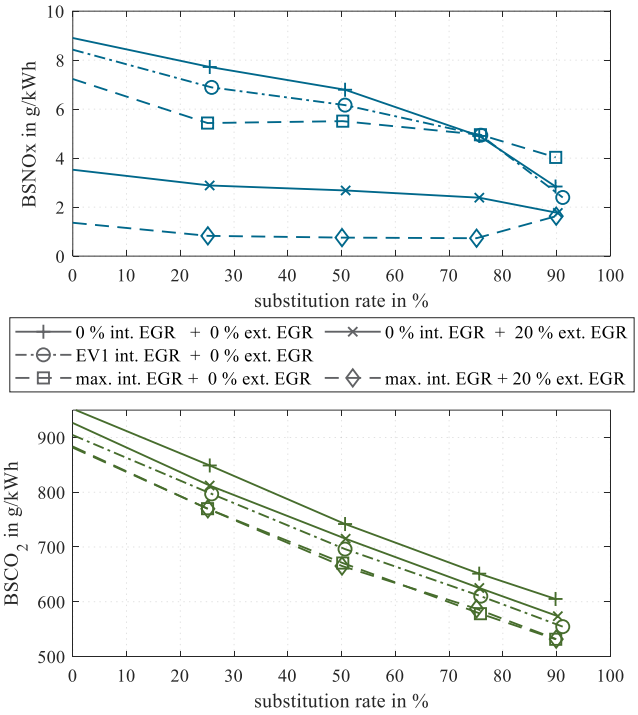

Figure 13. BSNOx and $BSCO_2$ emissions for internal and external EGR variation at substitution rates between 0 % and 90 % CNG share (1600 min^{-1}, 350 Nm)

While BDC pressure decreased with higher EGR rates, the exhaust manifold temperature increased (cf. Figure 14). This phenomenon is caused by the effect of lowering the cylinder charge mass due to pressure losses when using EGR. Also, the specific heat capacity is increased before combustion, which leads to a further reduction of the peak combustion temperature. However, due to the reduction of cylinder charge mass caused by EGR, this effect is mitigated and the absolute heat capacity needs to be considered. As a result, the exhaust gas temperatures increased with increasing EGR rates. Again, internal EGR had a larger impact on exhaust gas temperature and caused a more substantial increase compared to external EGR. Since the light-off temperature for methane catalysts is beyond 450 °C, an increase in exhaust gas temperature would be beneficial for the required exhaust gas aftertreatment [45].

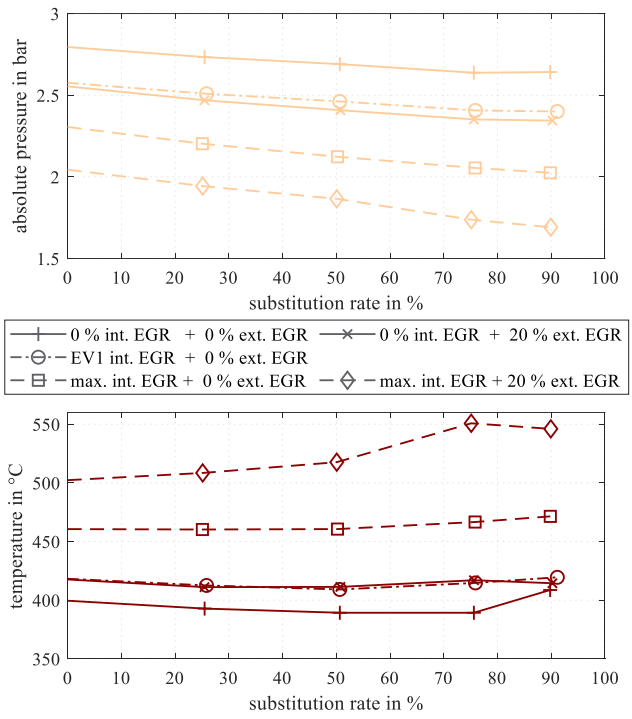

Figure 14. Bottom dead center pressure and exhaust temperature for internal and external EGR variation at substitution rates between 0 % and 90 % CNG share (1600 min^{-1}, 350 Nm)

The upper part of Figure 15 shows the apparent heat release rates for cylinder 4 at different EGR rates. The main difference in AHRR progression for the operation with and without internal EGR is that the transition from premixed combustion to a combination of mixing-controlled diffusion flame and flame front combustion is more pronounced. The green curve illustrates operation without internal EGR but with 20 % external EGR. The initial steep increase of the curve indicates premixed combustion before transitioning into a mixture of mixing-controlled diffusion flame and flame front combustion. This transition is marked by a brief decrease in AHRR. In operation with internal EGR, the transition is much smoother and cannot be determined precisely.

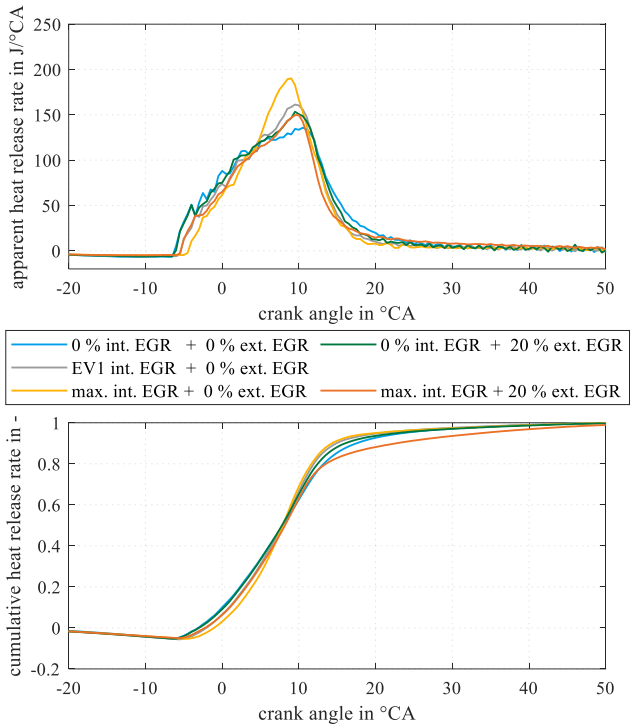

Figure 15. Apparent and cumulative heat release rates for cylinder 4 for variating EGR rates at 50 % CNG share (1600 min^{-1}, 350 Nm)

The combustion duration decreased when using EGR compared to operation without EGR. The case of maximum internal and 20 % external EGR stands out as an exception, primarily owing to a high residual gas content exceeding 40 %. The detailed discussion of the computed residual gas fractions is provided in the last paragraph of this section. Internal EGR considerably reduced the combustion duration, while the influence of external EGR on the combustion duration was less significant. The combustion duration and the ignition delay of the investigated operating points are shown in Figure 16. The ignition delay is prolonged with the use of external EGR, but the combination with internal EGR can mitigate this effect. Internal EGR even shortens the ignition delay in comparison to operation without EGR.

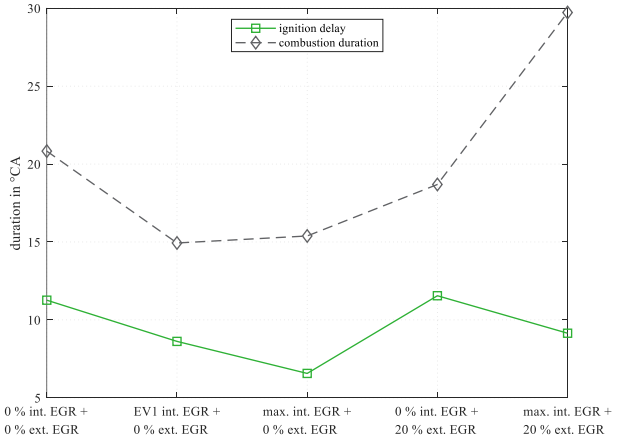

Figure 16. Ignition delay and combustion duration for internal and external EGR variation at 50 % CNG share (1600 min^{-1}, 350 Nm)

The effect of internal and external EGR on the calculated burned zone temperatures are shown in Figure 17. Internal EGR with the second event lift on exhaust valve 1 has only little influence on the burned zone temperature. The in-cylinder temperature before combustion onset is on a significantly higher level, though. The implementation of the second event lift on both exhaust valves lowers the burned zone temperature but exhibits a less rapid decrease. This correlation is more evident with the combination of external and internal EGR, resulting in a considerably prolonged phase with temperatures at an elevated level. When operating only with external EGR (without internal EGR), the initial temperature level is sustained for a more extended duration, and the subsequent temperature decrease is steeper in comparison to internal EGR.

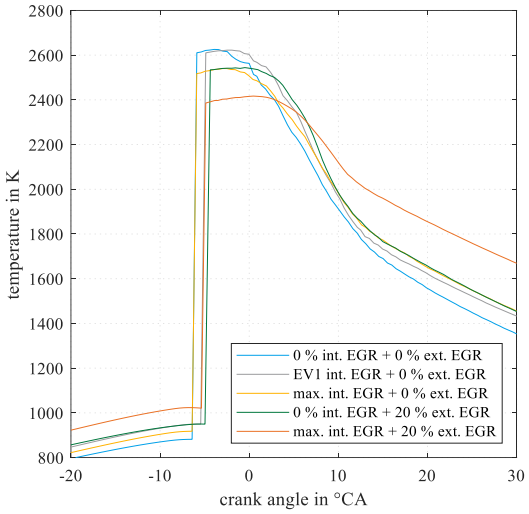

Figure 17. Effect of internal and external EGR on the progression of in-cylinder temperature of the burned zone according to TPA simulation at 50 % substitution rate (1600 min^{-1}, 350 Nm), calculated values

Figure 18 shows the air-fuel equivalence ratio as a function of the substitution rate in the upper diagram and BTE below. Both were investigated for different EGR rates. The air-fuel equivalence ratio decreased both with increasing EGR rate and CNG share. With the dual-fuel combustion mode, it was possible to achieve near-to-stochiometric combustion with a BTE of 38 %. As mentioned earlier, the BDC pressure decreased with increasing EGR, which resulted in a lower air-fuel equivalence ratio. The course of BDC pressure and air-fuel equivalence ratio were almost proportional since both depend on the inlet air mass flow which was also lowered with rising EGR rates. The trend of BTE is similar to that of the CO_2 emissions, which allows a direct conclusion on the efficiency, since both are directly influenced by the gas exchange loss, which decreased with increasing EGR rate, but more pronounced with internal than with external EGR. Therefore, the operating points with internal EGR also showed higher BTE than the comparable points with external EGR or a combination of both. The efficiency for the point with only one SE at 90 % substitution rate is not applicable for this analysis. At this point, THC and CO emissions showed a significant increase, leading to decreased BTE. The highest efficiency for 90 % substitution rate is achieved with max. int. EGR, while the efficiency for the combination of internal and external EGR is only 0.3 % lower, however.

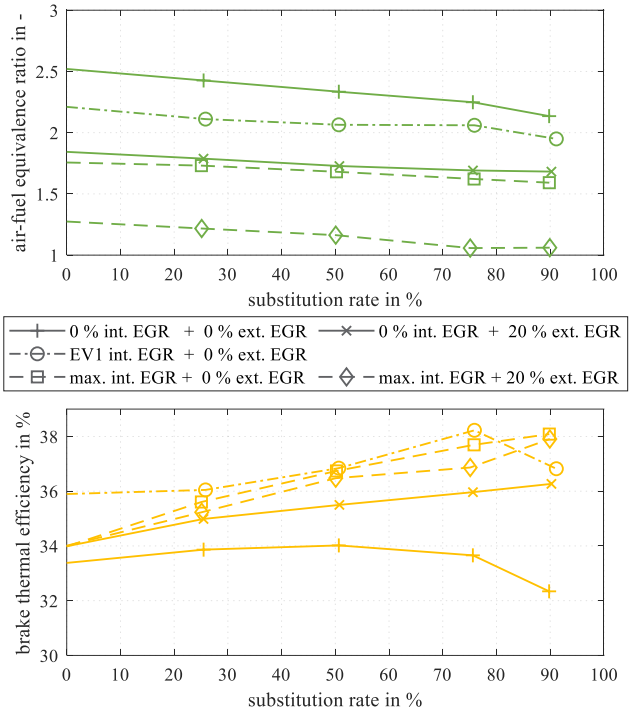

Figure 18. Air-fuel equivalence ratio and BTE for internal and external EGR variation for substitution rates between 0 % and 90 % CNG share (1600 min^{-1}, 350 Nm)

The total residual gas fractions at 50 % substitution rate (obtained through TPA) are shown in Figure 19. The corresponding exhaust valve lifts for the calculated residual gas fractions are shown in the lower part. EV1 int. EGR shows the valve lift of exhaust valve 1 while EV2 int. EGR shows the valve lift for exhaust valve 2. For the operating point max. int. EGR the second event lift is activated on both exhaust valves. As illustrated by Figure 1, the second event can only be reduced or switched off while at the same time reducing the main exhaust opening event with the current layout. Therefore, early exhaust valve closure before 360° CA is unavoidable when switching off the second event. This leads to a negative valve overlap and resulted in a residual gas content of almost 6 % in operation without EGR. By implementing the second event, the residual gas content could be increased to 19 % and up to 24 % with the second event lift active on both exhaust valves. On the other hand, with an external EGR rate of 20 %, the total residual gas content was 28 %. This percentage could be lifted to more than 40 % residual gas content after completion of gas exchange by combining external EGR with internal EGR on both exhaust valves. The residual gas in the combustion chamber displaced a part of the air, which resulted in the observed decrease in the formation of nitrogen oxides.

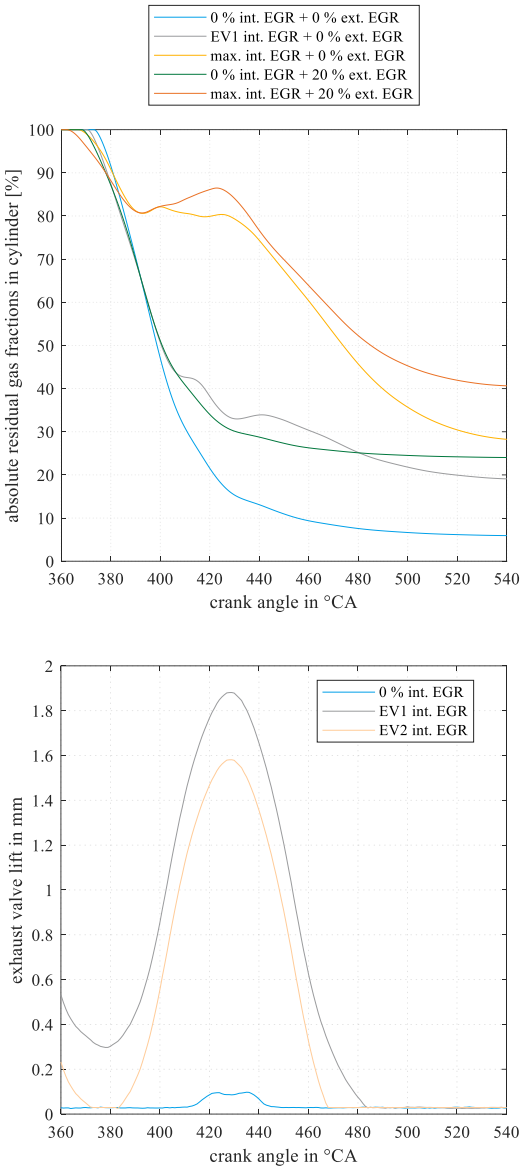

Figure 19. Effect of internal and external EGR on the in-cylinder calculated residual gas fractions during gas exchange according to TPA simulation at 50 % substitution rate (1600 min^{-1}, 350 Nm) and the corresponding exhaust valve lifts

Summary and Conclusions

The influence of external and internal EGR on a CNG-OME dual-fuel combustion engine has been investigated in this work. Since particulate emissions were found to be negligible throughout the investigations, the EGR rate was not limited by soot. As a result, it was possible to reach near-to-stochiometric combustion with a diesel engine in dual-fuel mode. The variation of EGR was carried out for different substitution rates to evaluate the impact of the CNG share. The investigations lead to the following conclusions:

- Raw THC and CO emissions rose significantly with increasing CNG substitution. However, the use of EGR could mitigate the influence of the higher CNG share. The THC emissions could therefore be reduced from 22.7 g/kWh to 4.4 g/kWh at a 90 % substitution rate during the investigations, while the CO emissions could be lowered from 13.6 g/kWh to 3.6 g/kWh, respectively.
- CO_2 emissions could be reduced drastically through the substitution by CNG and even further with the use of EGR. Starting at 0 % CNG substitution with around 950 g/kWh CO_2, 90 % CNG substitution rate resulted in 605 g/kWh. With the combination of internal and external EGR, CO_2 emissions decreased to 532 g/kWh, reflecting the corresponding increase in efficiency.
- NOx emissions decreased with increasing substitution rate and could be lowered further through EGR addition. EGR caused a rise in cylinder charge temperature and therefore a lower density of the charge, which resulted in a reduction of the pressure peak during combustion. NOx emissions could thus be lowered from 8.9 g/kWh to 1.6 g/kWh.
- The AHRR suggests that a two-phase combustion was taking place, starting with premixed combustion and then turning into a mixture of diffusion flame and flame front combustion, depending on the CNG substitution rate.

References

[1] REGULATION (EU) 2019/1242 of the EUROPEAN PARLIAMENT and of the COUNCIL of 20 June 2019 Setting CO 2 Emission Performance Standards for New Heavy-Duty Vehicles and Amending Regulations (EC) No 595/2009 and (EU) 2018/956 of the European Parliament and of the Council and Council Directive 96/53/EC. Accessed September 27, 2023. https://eur-lex.europa.eu/legal-content/de/TXT/?uri=CELEX%3A32019R1242

[2] Needell, Z. A., McNerney, J., Chang, M. T., and Trancik, J. E., “Potential for widespread electrification of personal vehicle travel in the United States.” 2016. *Nat Energy* 1 (9), https://doi.org/10.1038/nenergy.2016.112

[3] TFZ Technologie- und Förderzentrum, “HVO, BtL, E-Fuels.” Accessed September 29, 2023. https://www.tfz.bayern.de/biokraftstoffe/efuels/index.php

[4] Breuer, J., Scholten, J., Koj, J., Schorn, F., Fiebrandt, M., Samsun, R., Albus, R., Görner, K., Stolten, D., and Peters, R., “An Overview of Promising Alternative Fuels for Road, Rail, Air, and Inland Waterway Transport in Germany.” 2022. *Energies* 15 (4): p. 1443, https://doi.org/10.3390/en15041443

[5] Ueckerdt, F., Bauer, C., Dirnaichner, A., Everall, J., Sacchi, R., and Luderer, G., “Potential and risks of hydrogen-based e-fuels in climate change mitigation.” 2021. *Nat. Clim. Chang.* 11 (5): pp. 384–393, https://doi.org/10.1038/s41558-021-01032-7

[6] He, T., Pachfule, P., Wu, H., Xu, Q., and Chen, P., “Hydrogen carriers.” 2016. *Nat Rev Mater* 1 (12), https://doi.org/10.1038/natrevmats.2016.59

[7] Kramer, U., “Defossilizing the transportation sector. Options and requirements for Germany." 2018. Accessed September 29, 2023. https://www.fvv-net.de/fileadmin/Transfer/Downloads/FVV_Future_Fuels_Study_

report_Defossilizing_the_transportation_sector_R586_final_v.3_2019-06-14__EN.pdf

[8] Martin, J., and Boehman, A., “Mapping the combustion modes of a dual-fuel compression ignition engine.” 2022. *International Journal of Engine Research* 23 (9): pp. 1453–1474, https://doi.org/10.1177/14680874211018376

[9] Imran, S., Emberson, D. R., Diez, A., Wen, D. S., Crookes, R. J., and Korakianitis, T., “Natural gas fueled compression ignition engine performance and emissions maps with diesel and RME pilot fuels.” 2014. *Applied Energy* 124: pp. 354–365, https://doi.org/10.1016/j.apenergy.2014.02.067

[10] Hanson, R., Splitter, D., and Reitz, R. D., “Operating a Heavy-Duty Direct-Injection Compression-Ignition Engine with Gasoline for Low Emissions.", SAE Technical Paper 2009-01-1442 (2009), https://doi.org/10.4271/2009-01-1442

[11] Kassa, M., and Hall, C., “Dual-Fuel Combustion." 2019, *In: Paolo Carlucci, A. (eds), The Future of Internal Combustion Engines*. IntechOpen, https://doi.org/10.5772/intechopen.80570

[12] Damyanov, A., and Hofmann, P., “Operation of a diesel engine with intake manifold alcohol injection.” 2019. *Automot. Engine Technol.* 4 (1-2): pp. 17–28, https://doi.org/10.1007/s41104-019-00040-2

[13] van Basshuysen, Richard. *Handbuch Verbrennungsmotor: Grundlagen, Komponenten, Systeme, Perspektiven* 2015. With the assistance of F. Schäfer. 7th ed. ATZ/MTZ-Fachbuch Ser. Wiesbaden: Springer Vieweg. in Springer Fachmedien Wiesbaden GmbH

[14] Splitter, D., Reitz, R. D., and Hanson, R., “High Efficiency, Low Emissions RCCI Combustion by Use of a Fuel Additive.” 2010. *SAE Int. J. Fuels Lubr.* 3 (2): pp. 742–756, https://doi.org/10.4271/2010-01-2167

[15] Dempsey, A. B., Walker, N. R., Gingrich, E., and Reitz, R. D., “Comparison of Low Temperature Combustion Strategies for Advanced Compression Ignition Engines with a Focus on Controllability.” 2014. *Combustion Science and Technology* 186 (2): pp. 210–241, https://doi.org/10.1080/00102202.2013.858137

[16] Kokjohn, S. L., Hanson, R. M., Splitter, D. A., and Reitz, R. D., “Fuel reactivity controlled compression ignition (RCCI): a pathway to controlled high-efficiency clean combustion.” 2011. *International Journal of Engine Research* 12 (3): pp. 209–226, https://doi.org/10.1177/1468087411401548

[17] Bessonette, P. W., Schleyer, C. H., Duffy, K. P., Hardy, W. L., and Liechty, M. P., “Effects of Fuel Property Changes on Heavy-Duty HCCI Combustion.", SAE Technical Paper 2007-01-0191 (2007), https://doi.org/10.4271/2007-01-0191

[18] Hardy, W. L., and Reitz, R. D., “A Study of the Effects of High EGR, High Equivalence Ratio, and Mixing Time on Emissions Levels in a Heavy-Duty Diesel Engine for PCCI Combustion.", SAE Technical Paper 2006-01-0026 (2006), https://doi.org/10.4271/2006-01-0026

[19] Inagaki, K., Fuyuto, T., Nishikawa, K., Nakakita, K., and Sakata, I., “Dual-Fuel PCI Combustion Controlled by In-Cylinder Stratification of Ignitability.", SAE Technical Paper 2006-01-0028 (2006), https://doi.org/10.4271/2006-01-0028

[20] Kokjohn, S. L., Hanson, R. M., Splitter, D. A., and Reitz, R. D., “Experiments and Modeling of Dual-Fuel HCCI and PCCI Combustion Using In-Cylinder Fuel Blending.” 2009. *SAE Int. J. Engines* 2 (2): pp. 24–39, https://doi.org/10.4271/2009-01-2647

[21] Paykani, A., Kakaee, A.-H., Rahnama, P., and Reitz, R. D., “Progress and recent trends in reactivity-controlled compression ignition engines.” 2016. *International Journal of Engine Research* 17 (5): pp. 481–524, https://doi.org/10.1177/1468087415593013

[22] Yu, C., Wang, J., Wang, Z., and Shuai, S., “Comparative study on Gasoline Homogeneous Charge Induced Ignition (HCII) by diesel and Gasoline/Diesel Blend Fuels (GDBF) combustion.” 2013. *Fuel* 106: pp. 470–477, https://doi.org/10.1016/j.fuel.2012.10.068

[23] Chen, Y., Zhu, Z., Chen, Y., Huang, H., Zhu, Z., Lv, D., Pan, M., and Guo, X., “Study of injection pressure couple with EGR on combustion performance and emissions of natural gas-diesel dual-fuel engine.” 2020. *Fuel* 261: p. 116409, https://doi.org/10.1016/j.fuel.2019.116409

[24] Dev, S., Guo, H., Lafrance, S., and Liko, B., “An Experimental Study on the Effect of Exhaust Gas Recirculation on a Natural Gas-Diesel Dual-Fuel Engine.", SAE Technical Paper 2020-01-0310 (2020), https://doi.org/10.4271/2020-01-0310

[25] Gonzalez D, M. A., and Di Nunno, D., “Internal Exhaust Gas Recirculation for Efficiency and Emissions in a 4-Cylinder Diesel Engine.", SAE Technical Paper 2016-01-2184 (2016), https://doi.org/10.4271/2016-01-2184

[26] Shim, E. j., Park, H., and Bae, C., “Effects of Hot and Cooled EGR for HC Reduction in a Dual-Fuel Premixed Charge Compression Ignition Engine.", SAE Technical Paper 2018-01-1730 (2018), https://doi.org/10.4271/2018-01-1730

[27] Mueller, F., Guenthner, M., Weigel, A., and Thees, M., “Investigation of a Second Exhaust Valve Lift to Improve Combustion in a Methane - Diesel Dual-Fuel Engine.", SAE Technical Paper 2022-01-0466 (2022), https://doi.org/10.4271/2022-01-0466

[28] Pélerin, D., Gaukel, K., Härtl, M., Jacob, E., and Wachtmeister, G., “Potentials to simplify the engine system using the alternative diesel fuels oxymethylene ether OME1 and OME3−6 on a heavy-duty engine.” 2020. *Fuel* 259: p. 116231, https://doi.org/10.1016/j.fuel.2019.116231

[29] Jost, A.-K., Günthner, M., Müller, F., and Weigel, A., “Investigation of an Engine Concept for CNG-OME Dual Fuel Operation Using External and Internal EGR.", SAE Technical Paper 2022-32-0067 (2022), https://doi.org/10.4271/2022-32-0067

[30] Burger, J., Siegert, M., Ströfer, E., and Hasse, H., “Poly(oxymethylene) dimethyl ethers as components of tailored diesel fuel: Properties, synthesis and purification concepts.” 2010. *Fuel* 89 (11): pp. 3315–3319, https://doi.org/10.1016/j.fuel.2010.05.014

[31] Schmitz, N., Ströfer, E., Burger, J., and Hasse, H., “Conceptual Design of a Novel Process for the Production of Poly(oxymethylene) Dimethyl Ethers from Formaldehyde and Methanol.” 2017. *Ind. Eng. Chem. Res.* 56 (40): pp. 11519–11530, https://doi.org/10.1021/acs.iecr.7b02314

[32] Srna, A., Barro, C., Herrmann, K., Möri, F., Hutter, R., and Boulouchos, K., “POMDME as an Alternative Pilot Fuel for Dual-Fuel Engines: Optical Study in a RCEM and Application in an Automotive Size Dual-Fuel Diesel Engine.", SAE Technical Paper 2018-01-1734 (2018), https://doi.org/10.4271/2018-01-1734

[33] Hariharan, D., Partridge, K., Narayanan, A., Srinivasan, K., Krishnan, S. R., and Anandaraman, N., “Strategies for Reduced Engine-Out HC, CO, and NOx Emissions in Diesel-Natural Gas and POMDME-Natural Gas Dual-Fuel Engine.” 2022. *SAE Int. J. Adv. & Curr. Prac. in Mobility* 4 (4): pp. 1264–1278, https://doi.org/10.4271/2022-01-0460

[34] Duan, H., Jia, M., Bai, J., and Li, Y., “Potential of reactivity-controlled compression ignition with reverse reactivity stratification (R-RCCI) fueled with gasoline and polyoxymethylene dimethyl ethers (PODE n).” 2022. *International Journal of Engine Research* 23 (8): pp. 1308–1326, https://doi.org/10.1177/14680874211013667

[35] Mueller, F., and Guenthner, M., “Comparison of Premixed Fuel and Premixed Charge Operation for Propane-Diesel Dual-Fuel Combustion."SAE Technical Paper 2023-24-0059 (2023), https://doi.org/10.4271/2023-24-0059

[36] Buitkamp, T., Günthner, M., Müller, F., and Beutler, T., “A detailed study of a cylinder activation concept by efficiency loss analysis and 1D simulation.” 2020. *Automot. Engine Technol.* 5 (3-4): pp. 159–172, https://doi.org/10.1007/s41104-020-00070-1

[37] REGULATION (EU) 2016/1628 of the EUROPEAN PARLIAMENT and of the COUNCIL of 14 September 2016 on Requirements Relating to Gaseous and Particulate Pollutant Emission Limits and Type-Approval for Internal Combustion Engines for Non-Road Mobile Machinery, Amending Regulations (EU) No 1024/2012 and (EU) No 167/2013, and Amending and Repealing Directive 97/68/EC. Accessed October 06, 2023

[38] Oelschlegel, H. J., “Dieselmotorische Verbrennung." 2018, *In: Tschöke, H., Mollenhauer, K., and Maier, R. (eds), Handbuch Dieselmotoren*. Springer Fachmedien Wiesbaden, Wiesbaden, pp. 91–116, https://doi.org/10.1007/978-3-658-07697-9_9

[39] Thees, M., Buitkamp, T., Guenthner, M., and Pickel, P., “High Efficiency Diesel Engine Concept With Variable Valve Train and Cylinder Deactivation for Integration Into a Tractor." (2019), https://doi.org/10.1115/ICEF2019-7177

[40] Belgiorno, G., Di Blasio, G., and Beatrice, C., “Parametric study and optimization of the main engine calibration parameters and compression ratio of a methane-diesel dual fuel engine.” 2018. *Fuel* 222: pp. 821–840, https://doi.org/10.1016/j.fuel.2018.02.038

[41] Krishnasamy, A., Gupta, S. K., and Reitz, R. D., “Prospective fuels for diesel low temperature combustion engine applications: A critical review.” 2021. *International Journal of Engine Research* 22 (7): pp. 2071–2106, https://doi.org/10.1177/1468087420960857

[42] Kamimoto, T., and Bae, M., “High Combustion Temperature for the Reduction of Particulate in Diesel Engines." (1988), https://doi.org/10.4271/880423

[43] Eckert, P., and Rakowski, S., “Schadstoffbildung." 2019, *In: Merker, G. P. and Teichmann, R. (eds), Grundlagen Verbrennungsmotoren*. Springer Fachmedien Wiesbaden, Wiesbaden, pp. 943–977, https://doi.org/10.1007/978-3-658-23557-4_35

[44] Heywood, John B. *Internal Combustion Engine Fundamentals* 2018. Second revised edition. McGraw-Hill series in mechanical engineering. New York, Chicago, San Francisco und 9 andere: McGraw-Hill Education

[45] Lehtoranta, K., Koponen, P., Vesala, H., Kallinen, K., and Maunula, T., “Performance and Regeneration of Methane Oxidation Catalyst for LNG Ships.” 2021. *JMSE* 9 (2): p. 111, https://doi.org/10.3390/jmse9020111

Contact Information

Dipl.-Ing. Ann-Kathrin Jost

RPTU University of Kaiserslautern-Landau, Germany
Institute of Vehicle Propulsion Systems (LAF)
D-67663 Kaiserslautern/Germany

E-Mail: ann-kathrin.jost@mv.rptu.de

Acknowledgments

The work presented here was carried out within the framework of the project "CNG-OME Dual-Fuel Motorenkonzept", funded by the European Regional Development Fund (EFRE) and the Commercial Vehicle Cluster (CVC-Suedwest). The authors would like to express their gratitude for this funding.

Furthermore, the authors would like to thank the associated project partner John Deere for their support throughout the project.

Definitions/Abbreviations

AHRR	apparent heat release rate
BMEP	brake mean effective pressure
BTDC	before top dead center
CA	crank angle
CNG	compressed natural gas
CO	carbon monoxide
CO_2	carbon dioxide
COC	Center of combustion
CI	compression ignition
DAC	direct air capture
DFC	dual-fuel combustion
EGR	exhaust gas recirculation
HCCI	homogeneous charge compression ignition
HCII	homogeneous charge induced ignition
HRF	high reactivity fuel
HRR	heat release rate
LNG	liquefied natural gas
LRF	low reactivity fuel
MPI	multi point injection
NO_x	nitric oxide ($NO+NO_2$)
OME	polyoxymethylene ether
PCCI	premixed charge compression ignition
RCCI	reactivity controlled compression ignition
PFI	port fuel injection
SI	spark ignition
TDC	top dead center
THC	total hydrocarbons
TPA	three pressure analysis